

Quasi-symmetry Constrained Spin Ferromagnetism in Altermagnets

Mercè Roig,¹ Yue Yu,² Rune C. Ekman,¹ Andreas Kreisel,¹ Brian M. Andersen,¹ and Daniel F. Agterberg²

¹*Niels Bohr Institute, University of Copenhagen, DK-2100 Copenhagen, Denmark*

²*Department of Physics, University of Wisconsin–Milwaukee, Milwaukee, Wisconsin 53201, USA*

Altermagnets break time-reversal symmetry and their spin-orbit coupling (SOC) allow for an anomalous Hall effect (AHE) that depends on the direction of the Néel ordering vector. The AHE and the ferromagnetic spin moment share the same symmetry and hence are usually proportional. However, density functional theory (DFT) calculations find that the AHE exists with negligible ferromagnetic spin moment for some compounds, whereas it reaches sizable values for other altermagnets. By examining realistic minimal models for altermagnetism in which the DFT phenomenology is captured, we uncover a general SOC-enabled quasi-symmetry that provides a natural explanation for the amplitude of the ferromagnetic spin moment across the vast range of different altermagnetic materials. Additionally, we derive analytic expressions for the magnetic anisotropy energy, providing a simple means to identify the preferred Néel vector orientation for altermagnets.

Introduction.— The Hall effect has been a frontier theme in condensed matter physics for more than half a century. Fundamental understanding of the quantized Hall conductance and the anomalous Hall effect (AHE) has helped pave the way for topological classifications of quantum matter and the importance of Berry curvature in transport properties [1]. More recently, this has been generalized to nonlinear transport, which has been described in terms of multipoles of the quantum geometric tensor [2–7]. The discovery of altermagnetism (AM) and its associated large antiferromagnetic AHE is yet another testimony to this development [8–17], which may open new opportunities for devices utilizing dissipationless transport and spintronics technologies [5, 18–21].

The AHE in AM is only nonzero for certain directions of the Néel vector and in the presence of relativistic symmetry-lowering spin-orbit coupling (SOC). This, in addition, induces weak ferromagnetism (FM), which satisfies the same symmetry properties as the AHE [22, 23]. This implies that, in principle, FM and AHE share the same dependence on the orientation of the Néel vector [21, 24, 25]. However, from DFT it is found that the relative amplitude of the AHE transport coefficient and the FM spin moment depends strongly on the particular AM material under investigation. For example, for the materials RuO₂ and MnTe, DFT finds large AHE of 40 S/cm and 300 S/cm, respectively, while the possible associated FM spin moment is either vanishing for RuO₂ and very small of order 10⁻⁴μ_B per Mn for MnTe [17, 18, 26]. In the case of MnTe and RuO₂, weak FM was also reported experimentally [16, 27], though the AM ground state of the latter material is still debated [28, 29]. A weak FM spin moment has also been identified by DFT in CrSb [30]. By contrast, in other AM, such as FeSb₂, DFT finds a large AHE of 143 S/cm and a relatively larger FM moment [31, 32]. Similarly, the material RuF₄ has also been predicted by DFT to exhibit a large FM spin moment of 0.22 μ_B on the Ru sites [33].

The results highlighted above reveal that the interplay

between AHE and weak FM in AM materials is not well understood. To gain deeper insight into the weak FM properties of AM it is crucial to analyze the role of SOC using realistic models. Here, by examining realistic microscopic models for AM in which the DFT phenomenology is captured [34], we identify which AM states have a large SOC induced AHE but a small FM spin moment. In addition, we find that our model-based results are generally valid. Specifically, they apply to all microscopic theories in which AM appears as a consequence of the exchange interaction. To show this, we identify a general SOC-enabled quasi-symmetry [35, 36] that establishes for which AM symmetries the symmetry-allowed FM is large or vanishingly small. Finally, the presence of SOC in AM breaks the spin-space degeneracy and leads to a preferred direction for the Néel vector. For example, DFT calculations have revealed that the moments are out-of-plane in RuO₂ [15], while in MnTe, FeSb₂, Nb₂FeB₂ and Ta₂FeB₂ the moments are predicted to be in-plane [26, 31, 37]. By examining analytic expressions for the Landau coefficients derived from realistic microscopic models, we elucidate how the structure of SOC allows for the AM anisotropy energy to be understood.

Interplay between magnetization and Néel order.— Introducing \vec{N} as the Néel order and \vec{M} as the magnetization, the general form of the free energy density in the presence of SOC can be written as

$$F = \frac{a_N}{2} \vec{N}^2 + \frac{b_N}{4} \vec{N}^4 + \frac{a_M}{2} \vec{M}^2 - \vec{h} \cdot \vec{M} + c_{ij} M_i N_j + s_1 (N_x^2 - N_y^2) + s_2 (N_x^2 + N_y^2 - 2N_z^2), \quad (1)$$

where a_N , b_N , a_M and c_{ij} are temperature-dependent Landau coefficients, \vec{h} is an applied field, and s_1 and s_2 are the coefficients determining the magnetic anisotropy energy due to SOC. Note that the bilinear coupling between the two orders M_i and N_j is only allowed in the presence of SOC [22]. This free energy describes orthorhombic or higher-symmetry point groups, for monoclinic groups see the supplementary material (SM) [38].

TABLE I. Free energy invariant for the bilinear coupling between M_i and N_j in the presence of SOC, with P denoting the point group and Γ_N corresponding to the IR of the spin splitting in each point group. The last column specifies if the coupling is generated from the order parameter $\tau_z \sigma_i$, or a secondary order parameter is needed to obtain the coupling.

P	Γ_N	$f_{\Gamma_N}(\mathbf{k})$	Lowest order invariant	M_i linear in SOC
C_{2h}	B_g	$\alpha k_x k_z + \beta k_y k_z$	$\alpha_1 N_x M_z, \alpha_2 N_y M_z$ $\alpha_3 N_z M_y, \alpha_4 N_z M_x$	✓
D_{2h}	B_{1g}	$k_x k_y$	$\alpha_1 M_x N_y + \alpha_2 M_y N_x$	✓
D_{2h}	B_{2g}	$k_x k_z$	$\alpha_1 M_y N_z + \alpha_2 M_z N_y$	✓
D_{2h}	B_{3g}	$k_y k_z$	$\alpha_1 M_z N_x + \alpha_2 M_x N_z$	✓
C_{4h}	B_g	$\alpha(k_x^2 - k_y^2) + \beta k_x k_y$	$M_x N_y + M_y N_x,$ $M_x N_x - M_y N_y$	✗
D_{4h}	A_{2g}	$k_x k_y (k_x^2 - k_y^2)$	$M_x N_y - M_y N_x$	✓
D_{4h}	B_{1g}	$k_x^2 - k_y^2$	$M_x N_x - M_y N_y$	✗
D_{4h}	B_{2g}	$k_x k_y$	$M_x N_y + M_y N_x$	✗
D_{3d}	A_{2g}	$k_x k_z (k_x^2 - 3k_y^2)$	$M_x N_y - M_y N_x$	✓
C_{6h}	B_g	$\alpha k_y k_z (k_y^2 - 3k_x^2) + \beta k_x k_z (k_x^2 - 3k_y^2)$	$\alpha M_z N_y (3N_x^2 - N_y^2) + \beta M_z N_x (3N_y^2 - N_x^2)$	✗
D_{6h}	A_{2g}	$k_x k_y (k_x^2 - 3k_y^2) \times (k_y^2 - 3k_x^2)$	$M_x N_y - M_y N_x$	✓
D_{6h}	B_{1g}	$k_y k_z (3k_x^2 - k_y^2)$	$M_z N_y (3N_x^2 - N_y^2)$	✗
D_{6h}	B_{2g}	$k_x k_z (k_x^2 - 3k_y^2)$	$M_z N_x (N_x^2 - 3N_y^2)$	✗
O_h	A_{2g}	$k_x^4 (k_y^2 - k_z^2) + k_y^4 (k_z^2 - k_x^2) + k_z^4 (k_x^2 - k_y^2)$	$M_x N_x (N_y^2 - N_z^2) + M_y N_y (N_z^2 - N_x^2) + M_z N_z (N_x^2 - N_y^2)$	✗

The lowest order invariant coupling M_i and N_j can be determined from symmetry analysis. The magnetization \vec{M} belongs to the axial vector irreducible representation (IR) Γ_A , see SM [38]. In contrast, \vec{N} belongs to the IR $\Gamma_A \otimes \Gamma_N$, with Γ_N the IR denoting the symmetry of the AM spin splitting. Hence, a coupling of M_i and N_j exists if the direct product $\Gamma_A \otimes \Gamma_A \otimes \Gamma_N$ contains the IR transforming trivially under all point group operations or, equivalently, there is a free energy invariant if $\Gamma_A \otimes \Gamma_A$ contains Γ_N [22]. In Table I we provide the form of the free energy invariants considering the relevant point groups and symmetries for the spin splitting identified in Ref. [34]. Note that for C_{6h} , O_h and certain IRs Γ_N of D_{6h} , a bilinear coupling is not allowed, and therefore the coupling is of higher order. Following a similar procedure, the lowest-order coupling between the magnetization and the Néel vector can also be identified [38, 39], and is included in Table I. Hence, this implies that for MnTe and CrSb, which have point group D_{6h} and $\Gamma_N = B_{1g}$, the FM moment will be small, in agreement with Refs. [26, 30].

Microscopic models and secondary order parameters.

To investigate the dependence of the induced FM spin moment on the SOC strength, we consider the general form of the minimal model for AM from Ref. [34] with the normal state Hamiltonian

$$H_0 = \varepsilon_{0,\mathbf{k}} + t_{x,\mathbf{k}} \tau_x + t_{z,\mathbf{k}} \tau_z + \tau_y \vec{\lambda}_{\mathbf{k}} \cdot \vec{\sigma}, \quad (2)$$

where τ_i represent sublattice and σ_i spin degrees of freedom. The specific form of the parameters entering the model depends on the space group, the point group and the Wyckoff site symmetry. The inter-sublattice hopping term $t_{x,\mathbf{k}}$ exhibits the full symmetry of the point group. However, the crystal asymmetric hopping term $t_{z,\mathbf{k}}$ must exhibit a \mathbf{k} dependence that transforms as the non-trivial IR Γ_N since it describes the local symmetry breaking from multipole moments [34, 40, 41]. To study the interplay of the Néel order \vec{N} and the induced \vec{M} , we consider the perturbation

$$H' = \tau_z \vec{N} \cdot \vec{\sigma} + \vec{M} \cdot \vec{\sigma} \quad (3)$$

to the normal state Hamiltonian. We calculate the corrections to the normal state free energy close to the critical temperature as the magnetic order sets in by evaluating the loop expansion of the free energy. To second order it reads

$$F^{(2)} = \frac{1}{2\beta} \sum_{i\omega_n} \text{Tr}[G_0 H' G_0 H']. \quad (4)$$

Here, the bare Green's function projected to the band basis is given by

$$G_0(\mathbf{k}, i\omega_n) = \sum_{a=\pm} G_0^a(\mathbf{k}, i\omega_n) |u_{\mathbf{k}}^a\rangle \langle u_{\mathbf{k}}^a|, \quad (5)$$

where $G_0^{(\pm)}(\mathbf{k}, i\omega_n) = \frac{1}{i\omega_n - (\varepsilon_{0,\mathbf{k}} \pm \tilde{E}_{\mathbf{k}})}$ denotes the Green's function in the band basis, with the two-fold degenerate eigenenergies $E_{\mathbf{k}}^{\pm} = \varepsilon_{0,\mathbf{k}} \pm \tilde{E}_{\mathbf{k}}$ with $\tilde{E}_{\mathbf{k}} = \sqrt{t_{x,\mathbf{k}}^2 + t_{z,\mathbf{k}}^2 + \vec{\lambda}_{\mathbf{k}}^2}$. The projection operator $|u_{\mathbf{k}}^a\rangle \langle u_{\mathbf{k}}^a|$ in Eq. (5) transforms from sublattice basis onto band a at wavevector \mathbf{k} [38, 42].

To examine the bilinear coupling between \vec{N} and \vec{M} , we derive an expression for the coefficient c_{ij} in Eq. (1). The analytic expressions for the other coefficients in Eq. (1) can be found in the SM [38]. The quadratic free energy contribution in Eq. (4) coupling \vec{M} and \vec{N} is given by

$$F_{NM}^{(2)} = \frac{1}{\beta} \text{Tr} \left[\sum_{a,b,i\omega_n} G^a(\mathbf{k}, i\omega_n) G^b(\mathbf{k}, i\omega_n) \tau_z \vec{N} \cdot \vec{\sigma} P_{\mathbf{k}}^a \vec{M} \cdot \vec{\sigma} P_{\mathbf{k}}^b \right]. \quad (6)$$

Calculating the trace and performing the Matsubara frequency sum, we obtain

$$F_{NM}^{(2)} = 2 \sum_{\mathbf{k}} \frac{t_{x,\mathbf{k}}}{\tilde{E}_{\mathbf{k}}^2} L(\mathbf{k}) \vec{\lambda}_{\mathbf{k}} \cdot (\vec{M} \times \vec{N}), \quad (7)$$

with the function

$$L(\mathbf{k}) = \left. \frac{df(\varepsilon)}{d\varepsilon} \right|_{\varepsilon=E_{\mathbf{k}}^+} + \left. \frac{df(\varepsilon)}{d\varepsilon} \right|_{\varepsilon=E_{\mathbf{k}}^-} - \frac{2[f(E_{\mathbf{k}}^-) - f(E_{\mathbf{k}}^+)]}{E_{\mathbf{k}}^- - E_{\mathbf{k}}^+}, \quad (8)$$

incorporating the density of states and Lindhard term. The combination $(\vec{M} \times \vec{N})$ in Eq. (7) reveals that a nonzero invariant exists only if the antisymmetric direct product of the two axial IRs $[\Gamma_A \otimes \Gamma_A]_-$ contains Γ_N . In Table I we list whether the invariant can be generated to linear order of SOC, the antisymmetric product for the different point groups in detailed in the SM [38]. The SOC is expected to have a weak effect in AM [19], and therefore the induced magnetization will be vanishingly small when it is not generated to linear order. As seen from Table I, for the point group D_{4h} the SOC-linear invariant is only generated for $\Gamma_N = A_{2g}$. Focusing on crystals with rutile structure i.e. space group (SG) 136 and Wyckoff position 2a for the magnetic atoms as in RuO_2 , MnF_2 , NiF_2 , and CoF_2 , we have $\Gamma_N = B_{2g}$. Consequently, the induced \vec{M} is at least quadratic in SOC, as opposed to the material candidates Nb_2FeB_2 and Ta_2FeB_2 , which have $\Gamma_N = A_{2g}$. Notably, Table I also shows that the FM moment induced in orthorhombic materials (D_{2h}) is generally expected to be larger.

To further verify these points, in Fig. 1 we show the calculated $\vec{M} = \mu_B \sum_{a,\mathbf{k}} \langle u_{\mathbf{k}}^a | \vec{S} | u_{\mathbf{k}}^a \rangle f(E_{\mathbf{k}}^a)$ relevant for (a) rutile structure (D_{4h} , $\Gamma_N = B_{2g}$) and (b) FeSb_2 structure (D_{2h} , $\Gamma_N = B_{1g}$). As seen, the SOC-induced \vec{M} indeed scales quadratically (linearly) with the SOC strength for SG 136 (FeSb_2) and is significantly smaller for the band relevant for rutile AM compared to FeSb_2 . For the case of FeSb_2 we additionally compare the induced \vec{M} for the Néel vector along the x -axis and the y -axis in Fig. 1(b) to see if \vec{M} follows the predicted microscopic ($M_x N_y - M_y N_x$) result for the invariant. Indeed, even though M_x and M_y are not symmetry-related, they are of opposite sign and nearly identical in magnitude for this material. In summary, these results explicitly demonstrate the properties summarized in Table I, which can be applied to gain similar insight for many classes of AM materials.

Finally, we note that in order to understand the quadratic dependence of \vec{M} on SOC, when \vec{M} is not allowed to linear order, requires the inclusion of secondary order parameters [22]. Specifically, when AM order sets in, secondary order parameters are also induced by symmetry, and they can give rise to a finite coupling between the two orders \vec{M} and \vec{N} . Such secondary order parameters include other spin textures as well as a current loop order, see SM [38]. The free energy for a secondary order parameter \vec{O} can be written as

$$F = \gamma^{(1)} \vec{O}^2 + \gamma_{ij}^{(2)} N_i O_j + \gamma_{ij}^{(3)} M_i O_j, \quad (9)$$

which couples bilinearly to \vec{M} and \vec{N} . Thus, to higher order \vec{N} can also induce a magnetization \vec{M} through the secondary order parameter \vec{O} . Our minimal model suggests that in this case the FM spin moment is at least quadratic in SOC.

Quasi-symmetry protection of negligible FM.— It is pos-

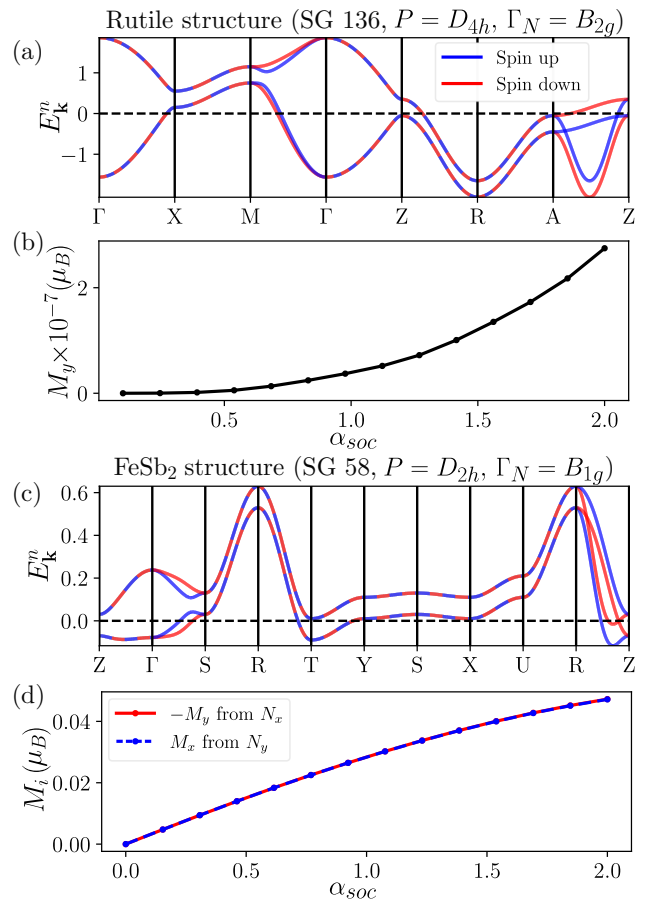


FIG. 1. Minimal model band structures and induced magnetization as a function of SOC strength for RuO_2 (a)-(b) vs FeSb_2 (c)-(d). We take $\vec{\lambda} = \alpha_{\text{soc}} \vec{\lambda}_0$, with $\vec{\lambda}_0 = (0.05, 0.05, 0.17)$ eV and $N_x = 0.2$ for RuO_2 , and $\vec{\lambda}_0 = (2.7, 6.6, 75)$ meV and $N_x = 0.05$ for FeSb_2 , both estimated from DFT results (see SM [38]). In agreement with Table I, \vec{M} is induced along the y axis for N_x , and scales quadratically (linearly) with the SOC strength for RuO_2 (FeSb_2). In (d) we show also the case with the Néel vector along the y -axis N_y , inducing $M_x \simeq -M_y$.

sible to understand the above results using the recently introduced concept of quasi-symmetry [35, 36], describing emergent approximate symmetries when certain terms in the Hamiltonian become negligible. Here we use SOC to generate our quasi-symmetry. Specifically, we consider the quasi-symmetry that emerges when two of the SOC components (λ_x , λ_y , or λ_z) vanish, as illustrated in Fig. 2 for a tetragonal system. This is relevant for the Landau coefficients since the SOC-linear contributions can be expressed as a linear combination of $\lambda_{x,y,z}$. For example, we consider that the λ_z -linear contribution is non-zero when the other two SOC terms are neglected. In that case, the normal state Hamiltonian gains additional symmetries, i.e., quasi-symmetries. Importantly, whether the λ_z -linear contribution to the Landau coeffi-

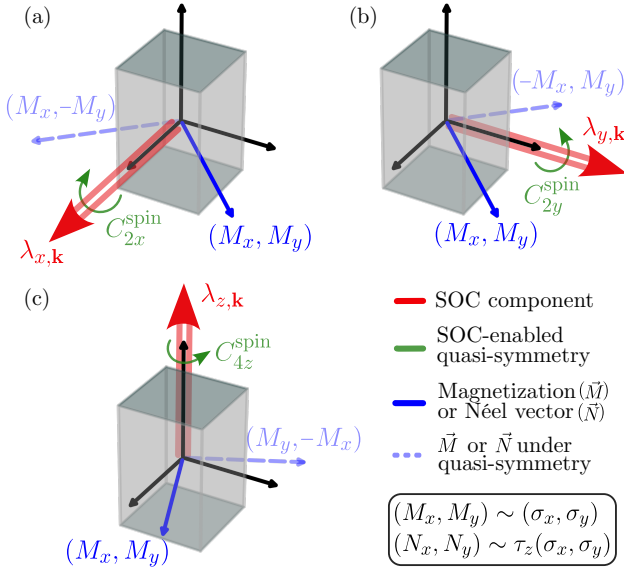


FIG. 2. SOC-enabled quasi-symmetry in a tetragonal system when only a single SOC component (a) $\lambda_{x,\mathbf{k}}$, (b) $\lambda_{y,\mathbf{k}}$ or (c) $\lambda_{z,\mathbf{k}}$ is present. The quasi-symmetry acts only in spin space, transforming the magnetization \vec{M} and the spin components of the Néel vector \vec{N} in the same way.

cient is permitted depends not only on the intrinsic symmetries of the crystal, but also on these emergent quasi-symmetries [35, 36].

Here, we apply this to the Landau coefficients of $M_x N_y$ and $M_y N_x$. When only λ_x (λ_y) SOC is present, the normal state Hamiltonian acquires an additional two-fold spin rotational symmetry C_{2x}^{spin} (C_{2y}^{spin}), see Fig. 2(a) (Fig. 2(b)), which prohibits λ_x (or λ_y)-linear contribution to these two Landau coefficients. When only λ_z is present, a relevant quasi-symmetry is 4-fold spin rotational symmetry C_{4z}^{spin} , as seen from Fig. 2(c). Under this symmetry, the SOC-linear contribution to $M_x N_y$ and $M_y N_x$ coefficients must have opposite sign. This behavior is universal and applies to any space group, regardless of whether it has intrinsic 4-fold rotational symmetry, as demonstrated in Fig. 1(b) for FeSb₂. In structures with SG 136, however, its intrinsic tetragonal crystal symmetries force these two coefficients to be identical at all orders of SOC. Consequently, the SOC-linear contribution must vanish, as shown in Fig. 1(a). The complete discussion on other space groups can be found in SM [38]. Hence, the SOC enabled quasi-symmetry demonstrates that the microscopic model leads to a general result, and naturally explains when the FM spin moment is large or small depending on the AM symmetry. The only assumption on the microscopic Hamiltonian that underlies this analysis is that AM is an instability purely in the spin-channel, that is, it is driven only by exchange interactions without any orbital angular momentum contribution.

Anomalous Hall effect.— In the SM we provide a de-

tailed analysis of the AHE. There are two main conclusions; the first is that it is generically nonzero when allowed by symmetry and the second is that it is dominated by the following term in the Berry curvature [34],

$$\Omega_{\alpha,\beta,ij}^{(N_x)} = \frac{1}{2E_{\alpha,\beta}^3} \sum_{m,n=i,j} \varepsilon_{mn} \left[(N_x + \beta|t_{z,\mathbf{k}}|) \partial_m \lambda_{x,\mathbf{k}} \partial_n t_{x,\mathbf{k}} + \text{sgn}(t_{z,\mathbf{k}}) \beta t_{x,\mathbf{k}} \partial_m t_{z,\mathbf{k}} \partial_n \lambda_{x,\mathbf{k}} + \text{sgn}(t_{z,\mathbf{k}}) \beta \lambda_{x,\mathbf{k}} \partial_m t_{x,\mathbf{k}} \partial_n t_{z,\mathbf{k}} \right], \quad (10)$$

where the dispersion is $E_{\alpha=\pm,\beta=\pm} = \alpha \left(N_x^2 + \tilde{E}_{\mathbf{k}}^2 + \beta 2N_x \sqrt{t_{z,\mathbf{k}}^2 + \lambda_{y,\mathbf{k}}^2 + \lambda_{z,\mathbf{k}}^2} \right)^{1/2}$. This term reveals that it is the SOC component parallel to the Néel vector that determines the AHE. This relationship between the SOC direction and non-vanishing AHE can also be understood using SOC-based quasi-symmetry arguments like those given above. Specifically, the AHE measures current and voltage response, and hence is even under spin-rotational symmetries. For the Néel order along \hat{x} , when only the λ_y (λ_z) SOC is kept, the Néel order is odd (under the resulting quasi-spin-rotational symmetry C_{2y}^{spin} (C_{2z}^{spin})). This prevents a λ_y (λ_z)-linear SOC contribution to the AHE. When only the λ_x SOC is kept, the Néel order is even under the resulting C_{2x}^{spin} symmetry, and therefore the λ_x -linear contribution to AHE is allowed by the quasi-symmetry. It naturally follows that the AHE is given by the SOC component that is parallel to the Néel vector. We note that this quasi-symmetry argument also applies to ferromagnetic order and this is confirmed by explicit microscopic calculations in the SM [38].

Magnetic anisotropy energy.— The presence of SOC leads to a preferred direction for the Néel vector. As seen from the free energy in Eq. (1), this is captured by the s_1 and s_2 Landau coefficients. Thus, deriving analytic expressions for these coefficients from the microscopic models is useful to provide insight into the easy axis direction. Using the general microscopic model in Eq. (2) and focusing on the quadratic free energy correction due to SOC (see Eq. (4)), the coefficients can be written as

$$s_1 = -\frac{1}{2} \sum_{\mathbf{k}} \frac{\lambda_{x,\mathbf{k}}^2 - \lambda_{y,\mathbf{k}}^2}{\tilde{E}_{\mathbf{k}}^2} L(\mathbf{k}), \quad (11)$$

$$s_2 = -\frac{1}{6} \sum_{\mathbf{k}} \frac{\lambda_{x,\mathbf{k}}^2 + \lambda_{y,\mathbf{k}}^2 - 2\lambda_{z,\mathbf{k}}^2}{\tilde{E}_{\mathbf{k}}^2} L(\mathbf{k}), \quad (12)$$

with the function $L(\mathbf{k})$ defined in Eq. (8). The sign of these coefficients fixes the easy axis for a specific AM material. For instance, focusing on SG 136, $\lambda_{z,\mathbf{k}}$ can be ignored as it is smaller than $\lambda_{x,\mathbf{k}}$ and $\lambda_{y,\mathbf{k}}$ [34]. Hence, in general we expect that $s_2 > 0$ and, as a consequence, the easy axis is out of plane. However, Eqs. (11)-(12) also reveal that the moment direction may switch depending on

the Fermi energy. In particular, when the Lindhard function (interband term in $L(\mathbf{k})$) dominates over the density of states (intra-band term), $L(\mathbf{k})$ can change sign leading to $s_2 < 0$ and in-plane moment orientation. The switch of the AM moments as a function of the Fermi energy from the c -axis to the in-plane direction has been reported in Ref. [15] for RuO_2 . As shown in the SM section, calculations of s_1 and s_2 for a minimal model of RuO_2 indeed yield $s_1 = 0$, $s_2 > 0$. In addition, application to FeSb_2 reveal that $s_1 > 0$, $s_2 < 0$, i.e. moments aligned along the in-plane y -axis, in agreement with DFT studies [31]. A systematic application of the magnetic anisotropy energy based on Eqs. (11)-(12) to other AM is beyond the scope of this work, and constitute an interesting future project.

Conclusions.— In summary we have applied recently-developed realistic microscopic models for AM to derive relevant Landau coefficients of the free energy, focusing on the coupling between magnetization and Néel order, and magnetic anisotropy energies. The results explain an observed strong material-dependence of the SOC-induced weak FM. We stress that the weak FM described in this work refers to the spin moment. For materials where this moment is forbidden to linear order, e.g. the rutiles, secondary orders become relevant, and the orbital magnetic moment may also yield contributions to the small but finite net magnetization [18, 43]. Finally, we discovered a general quasi-symmetry enabled by the SOC that allows to determine for which AM symmetries the induced FM spin moment is large or vanishingly small.

Acknowledgements.— M. R. acknowledges support from the Novo Nordisk Foundation grant NNF20OC0060019. A. K. acknowledges support by the Danish National Committee for Research Infrastructure (NUFI) through the ESS-Lighthouse Q-MAT. D. F. A. and Y. Y. were supported by the National Science Foundation Grant No. DMREF 2323857.

-
- [1] Naoto Nagaosa, Jairo Sinova, Shigeki Onoda, A. H. MacDonald, and N. P. Ong, “Anomalous Hall effect,” *Rev. Mod. Phys.* **82**, 1539–1592 (2010).
- [2] Inti Sodemann and Liang Fu, “Quantum Nonlinear Hall Effect Induced by Berry Curvature Dipole in Time-Reversal Invariant Materials,” *Phys. Rev. Lett.* **115**, 216806 (2015).
- [3] Anyuan Gao, Yu-Fei Liu, Jian-Xiang Qiu, Barun Ghosh, Thaís V. Trevisan, Yugo Onishi, Chaowei Hu, Tiema Qian, Hung-Ju Tien, Shao-Wen Chen, Mengqi Huang, Damien Bérubé, Houchen Li, Christian Tzschaschel, Thao Dinh, *et al.*, “Quantum metric nonlinear Hall effect in a topological antiferromagnetic heterostructure,” *Science* **381**, 181–186 (2023).
- [4] Daniel Kaplan, Tobias Holder, and Binghai Yan, “Unification of Nonlinear Anomalous Hall Effect and Nonreciprocal Magnetoresistance in Metals by the Quantum Geometry,” *Phys. Rev. Lett.* **132**, 026301 (2024).
- [5] Yuan Fang, Jennifer Cano, and Sayed Ali Akbar Ghorashi, “Quantum Geometry Induced Nonlinear Transport in Altermagnets,” *Phys. Rev. Lett.* **133**, 106701 (2024).
- [6] Z. Z. Du, Hai-Zhou Lu, and X. C. Xie, “Nonlinear Hall effects,” *Nature Reviews Physics* **3**, 744–752 (2021).
- [7] Naizhou Wang, Daniel Kaplan, Zhaowei Zhang, Tobias Holder, Ning Cao, Aifeng Wang, Xiaoyuan Zhou, Feifei Zhou, Zhengzhi Jiang, Chusheng Zhang, Shihao Ru, Hongbing Cai, Kenji Watanabe, Takashi Taniguchi, Binghai Yan, and Weibo Gao, “Quantum-metric-induced nonlinear transport in a topological antiferromagnet,” *Nature* **621**, 487–492 (2023).
- [8] Suyoung Lee, Sangjae Lee, Saegyeol Jung, Jiwon Jung, Donghan Kim, Yeonjae Lee, Byeongjun Seok, Jaeyoung Kim, Byeong Gyu Park, Libor Šmejkal, Chang-Jong Kang, and Changyoung Kim, “Broken Kramers Degeneracy in Altermagnetic MnTe,” *Phys. Rev. Lett.* **132**, 036702 (2024).
- [9] J. Krempaský, L. Šmejkal, S. W. D’Souza, M. Hajlaoui, G. Springholz, K. Uhlířová, F. Alarab, P. C. Constantinou, V. Strocov, D. Usanov, W. R. Pudelko, R. González-Hernández, A. Birk Hellenes, Z. Jansa, H. Reichlová, Z. Šobán, R. D. Gonzalez Betancourt, P. Wadley, J. Sinova, D. Krieger, J. Minár, J. H. Dil, and T. Jungwirth, “Altermagnetic lifting of Kramers spin degeneracy,” *Nature* **626**, 517–522 (2024).
- [10] T. Osumi, S. Souma, T. Aoyama, K. Yamauchi, A. Honma, K. Nakayama, T. Takahashi, K. Ohgushi, and T. Sato, “Observation of a giant band splitting in altermagnetic MnTe,” *Phys. Rev. B* **109**, 115102 (2024).
- [11] Cong Li, Mengli Hu, Zhilin Li, Yang Wang, Wanyu Chen, Balasubramanian Thiagarajan, Mats Leandersson, Craig Polley, Timur Kim, Hui Liu, Cosma Fulga, Maia G. Vergniory, Oleg Janson, Oscar Tjernberg, and Jeroen van den Brink, “Topological Weyl Altermagnetism in CrSb,” *arXiv* (2024), 10.48550/arXiv.2405.14777, 2405.14777.
- [12] Guowei Yang, Zhanghuan Li, Sai Yang, Jiyuan Li, Hao Zheng, Weifan Zhu, Ze Pan, Yifu Xu, Saizheng Cao, Wenxuan Zhao, Anupam Jana, Jiawen Zhang, Mao Ye, Yu Song, Lun-Hui Hu, Lexian Yang, Jun Fujii, Ivana Vobornik, Ming Shi, Huiqiu Yuan, Yongjun Zhang, Yuanfeng Xu, and Yang Liu, “Three-dimensional mapping and electronic origin of large altermagnetic splitting near Fermi level in CrSb,” *arXiv* (2024), 10.48550/arXiv.2405.12575, 2405.12575.
- [13] Sonka Reimers, Lukas Odenbreit, Libor Šmejkal, Vladimir N. Strocov, Procopios Constantinou, Anna B. Hellenes, Rodrigo Jaeschke Ubiergo, Warley H. Campos, Venkata K. Bharadwaj, Atasi Chakraborty, Thibaud Denneulin, Wen Shi, Rafal E. Dunin-Borkowski, Suvadip Das, Mathias Kläui, Jairo Sinova, and Martin Jourdan, “Direct observation of altermagnetic band splitting in CrSb thin films,” *Nat. Commun.* **15**, 1–7 (2024).
- [14] Jianyang Ding, Zhicheng Jiang, Xiuhua Chen, Zicheng Tao, Zhengtai Liu, Tongrui Li, Jishan Liu, Jianping Sun, Jinguang Cheng, Jiayu Liu, Yichen Yang, Runfeng Zhang, Liwei Deng, Wenchuan Jing, Yu Huang, Yuming Shi, Mao Ye, Shan Qiao, Yilin Wang, Yanfeng Guo, Donglai Feng, and Dawei Shen, “Large Band Splitting in g -Wave Altermagnet CrSb,” *Phys. Rev. Lett.* **133**, 206401 (2024).
- [15] Zexin Feng, Xiaorong Zhou, Libor Šmejkal, Lei Wu,

- Zengwei Zhu, Huixin Guo, Rafael González-Hernández, Xiaoning Wang, Han Yan, Peixin Qin, Xin Zhang, Haojiang Wu, Hongyu Chen, Ziang Meng, Li Liu, Zhengcai Xia, Jairo Sinova, Tomáš Jungwirth, and Zhiqi Liu, “An anomalous Hall effect in altermagnetic ruthenium dioxide,” *Nat. Electron.* **5**, 735–743 (2022).
- [16] K. P. Kluczyk, K. Gas, M. J. Grzybowski, P. Skupiński, M. A. Borysiewicz, T. Fas, J. Suffczyński, J. Z. Domagala, K. Graszka, A. Mycielski, M. Baj, K. H. Ahn, K. Výborný, M. Sawicki, and M. Gryglas-Borysiewicz, “Coexistence of anomalous Hall effect and weak magnetization in a nominally collinear antiferromagnet MnTe,” *Phys. Rev. B* **110**, 155201 (2024).
- [17] R. D. Gonzalez Betancourt, J. Zubáč, R. Gonzalez-Hernandez, K. Geishendorf, Z. Šobáň, G. Springholz, K. Olejník, L. Šmejkal, J. Sinova, T. Jungwirth, S. T. B. Goennenwein, A. Thomas, H. Reichlová, J. Železný, and D. Krieger, “Spontaneous Anomalous Hall Effect Arising from an Unconventional Compensated Magnetic Phase in a Semiconductor,” *Phys. Rev. Lett.* **130**, 036702 (2023).
- [18] Libor Šmejkal, Rafael González-Hernández, T. Jungwirth, and J. Sinova, “Crystal time-reversal symmetry breaking and spontaneous Hall effect in collinear antiferromagnets,” *Sci. Adv.* **6** (2020), 10.1126/sciadv.aaz8809.
- [19] Libor Šmejkal, Jairo Sinova, and Tomas Jungwirth, “Beyond Conventional Ferromagnetism and Antiferromagnetism: A Phase with Nonrelativistic Spin and Crystal Rotation Symmetry,” *Phys. Rev. X* **12**, 031042 (2022).
- [20] Libor Šmejkal, Jairo Sinova, and Tomas Jungwirth, “Emerging Research Landscape of Altermagnetism,” *Phys. Rev. X* **12**, 040501 (2022).
- [21] Libor Šmejkal, Allan H. MacDonald, Jairo Sinova, Satoru Nakatsuji, and Tomas Jungwirth, “Anomalous Hall antiferromagnets,” *Nat. Rev. Mater.* **7**, 482–496 (2022).
- [22] Paul A. McClarty and Jeffrey G. Rau, “Landau Theory of Altermagnetism,” *Phys. Rev. Lett.* **132**, 176702 (2024).
- [23] Rui-Chun Xiao, Hui Li, Hui Han, Wei Gan, Mengmeng Yang, Ding-Fu Shao, Shu-Hui Zhang, Yang Gao, Mingliang Tian, and Jianhui Zhou, “Anomalous-Hall Neel textures in altermagnetic materials,” *arXiv* (2024), 10.48550/arXiv.2411.10147, 2411.10147.
- [24] Rafael M. Fernandes, Vanuildo S. de Carvalho, Turan Birol, and Rodrigo G. Pereira, “Topological transition from nodal to nodeless Zeeman splitting in altermagnets,” *Phys. Rev. B* **109**, 024404 (2024).
- [25] Sang-Wook Cheong and Fei-Ting Huang, “Altermagnetism with non-collinear spins,” *npj Quantum Mater.* **9**, 1–6 (2024).
- [26] Igor I. Mazin, “Origin of the gossamer ferromagnetism in MnTe,” *arXiv* (2024), 10.48550/arXiv.2407.14389, 2407.14389.
- [27] T. Berlijn, P. C. Snijders, O. Delaire, H.-D. Zhou, T. A. Maier, H.-B. Cao, S.-X. Chi, M. Matsuda, Y. Wang, M. R. Koehler, P. R. C. Kent, and H. H. Weitering, “Itinerant Antiferromagnetism in RuO₂,” *Phys. Rev. Lett.* **118**, 077201 (2017).
- [28] M. Hiraishi, H. Okabe, A. Koda, R. Kadono, T. Muroi, D. Hirai, and Z. Hiroi, “Nonmagnetic Ground State in RuO₂ Revealed by Muon Spin Rotation,” *Phys. Rev. Lett.* **132**, 166702 (2024).
- [29] Philipp Keßler, Laura Garcia-Gassull, Andreas Suter, Thomas Prokscha, Zaher Salman, Dmitry Khalyavin, Pascal Manuel, Fabio Orlandi, Igor I. Mazin, Roser Valentí, and Simon Moser, “Absence of magnetic order in RuO₂: insights from μ SR spectroscopy and neutron diffraction,” *arXiv* (2024), 10.48550/arXiv.2405.10820, 2405.10820.
- [30] Carmine Autieri, Raghottam M. Sattigeri, Giuseppe Cuono, and Amar Fakhredine, “Staggered Dzyaloshinskii-Moriya inducing weak ferromagnetism in centrosymmetric altermagnets and weak ferrimagnetism in noncentrosymmetric altermagnets,” *arXiv* (2023), 10.48550/arXiv.2312.07678, 2312.07678.
- [31] Igor I. Mazin, Klaus Koepernik, Michelle D. Johannes, Rafael González-Hernández, and Libor Šmejkal, “Prediction of unconventional magnetism in doped FeSb₂,” *Proc. Natl. Acad. Sci. U.S.A.* **118**, e2108924118 (2021).
- [32] Lotan Attias, Alex Levchenko, and Maxim Khodas, “Intrinsic anomalous hall effect in altermagnets,” *Phys. Rev. B* **110**, 094425 (2024).
- [33] Marko Milivojević, Marko Orozović, Silvia Picozzi, Martin Gmitra, and Srđan Stavrić, “Interplay of altermagnetism and weak ferromagnetism in two-dimensional RuF₄,” *2D Mater.* **11**, 035025 (2024).
- [34] Mercè Roig, Andreas Kreisel, Yue Yu, Brian M. Andersen, and Daniel F. Agterberg, “Minimal models for altermagnetism,” *Phys. Rev. B* **110**, 144412 (2024).
- [35] Jiayu Li, Ao Zhang, Yuntian Liu, and Qihang Liu, “Group Theory on Quasisymmetry and Protected Near Degeneracy,” *Phys. Rev. Lett.* **133**, 026402 (2024).
- [36] Chunyu Guo, Lunhui Hu, Carsten Putzke, Jonas Diaz, Xiangwei Huang, Kaustuv Manna, Feng-Ren Fan, Chandra Shekhar, Yan Sun, Claudia Felser, Chaoxing Liu, B. Andrei Bernevig, and Philip J. W. Moll, “Quasisymmetry-protected topology in a semi-metal,” *Nature Physics* **18**, 813–818 (2022).
- [37] Xiao-Yao Hou, Huan-Cheng Yang, Zheng-Xin Liu, Peng-Jie Guo, and Zhong-Yi Lu, “Large intrinsic anomalous Hall effect in both Nb₂FeB₂ and Ta₂FeB₂ with collinear antiferromagnetism,” *Phys. Rev. B* **107**, L161109 (2023).
- [38] Mercè Roig, Yue Yu, Rune C. Ekman, Andreas Kreisel, Brian M. Andersen, and Daniel F. Agterberg, “Supplementary Material for: Quasi-symmetry Constrained Spin Ferromagnetism in Altermagnets,”.
- [39] Matthias Hecker, Anant Rastogi, Daniel F. Agterberg, and Rafael M. Fernandes, “Classification of electronic nematicity in three-dimensional crystals and quasicrystals,” *Phys. Rev. B* **109**, 235148 (2024).
- [40] Satoru Hayami, Megumi Yatsushiro, Yuki Yanagi, and Kusunose Hiroaki, “Classification of atomic-scale multipoles under crystallographic point groups and application to linear response tensors,” *Phys. Rev. B* **98**, 165110 (2018).
- [41] Sayantika Bhowal and Nicola A. Spaldin, “Ferroically Ordered Magnetic Octupoles in *d*-Wave Altermagnets,” *Phys. Rev. X* **14**, 011019 (2024).
- [42] Ansgar Graf and Frédéric Piéchon, “Berry curvature and quantum metric in *N*-band systems: An eigenprojector approach,” *Phys. Rev. B* **104**, 085114 (2021).
- [43] Daegeun Jo, Dongwook Go, Yuriy Mokrousov, Peter M. Oppeneer, Sang-Wook Cheong, and Hyun-Woo Lee, “Weak Ferromagnetism in Altermagnets from Alternating *g*-Tensor Anisotropy,” *arXiv* (2024), 10.48550/arXiv.2410.17386, 2410.17386.

Supplementary Material for: "Quasi-symmetry Constrained Spin Ferromagnetism in Altermagnets"

Mercè Roig,¹ Yue Yu,² Rune C. Ekman,¹ Andreas Kreisel,¹ Brian M. Andersen,¹ and Daniel F. Agterberg²

¹*Niels Bohr Institute, University of Copenhagen, DK-2100 Copenhagen, Denmark*

²*Department of Physics, University of Wisconsin–Milwaukee, Milwaukee, Wisconsin 53201, USA*

In this supplementary material, we provide details on supporting derivations, resulting analytical expressions for all coefficients in the free energy, extended (quasi)-symmetry analyses, examples of secondary order parameters, general analytic expressions for the Berry curvature and a detailed analysis of the magnetic anisotropy energy.

S1. GENERAL FREE ENERGY IN THE PRESENCE OF SPIN-ORBIT COUPLING

In the main text we include the form of the free energy for orthorhombic and higher-symmetry groups. In the case of monoclinic groups, there are additional terms due to the lower crystal symmetry, and therefore the free energy can generally be written as

$$f = \frac{a_N}{2} \vec{N}^2 + \frac{b_N}{4} \vec{N}^4 + \frac{a_M}{2} \vec{M}^2 - \vec{h} \cdot \vec{M} + c_{ij} M_i N_j + s_1 (N_x^2 - N_y^2) + s_2 (N_x^2 + N_y^2 - 2N_z^2) + s_3 N_x N_y + s_4 N_x N_z + s_5 N_y N_z, \quad (\text{S1})$$

where the coefficients s_3 , s_4 and s_5 can also be calculated from the general microscopic model and are given by

$$s_3 = -2 \sum_{\mathbf{k}} \frac{\lambda_{x,\mathbf{k}} \lambda_{y,\mathbf{k}}}{\tilde{E}_{\mathbf{k}}^2} L(\mathbf{k}), \quad (\text{S2})$$

$$s_4 = -2 \sum_{\mathbf{k}} \frac{\lambda_{x,\mathbf{k}} \lambda_{z,\mathbf{k}}}{\tilde{E}_{\mathbf{k}}^2} L(\mathbf{k}), \quad (\text{S3})$$

$$s_5 = -2 \sum_{\mathbf{k}} \frac{\lambda_{y,\mathbf{k}} \lambda_{z,\mathbf{k}}}{\tilde{E}_{\mathbf{k}}^2} L(\mathbf{k}). \quad (\text{S4})$$

with the function $L(\mathbf{k}) = \frac{df(\varepsilon)}{d\varepsilon} \Big|_{\varepsilon=E_{\mathbf{k}}^+} + \frac{df(\varepsilon)}{d\varepsilon} \Big|_{\varepsilon=E_{\mathbf{k}}^-} - \frac{2[f(E_{\mathbf{k}}^-) - f(E_{\mathbf{k}}^+)]}{E_{\mathbf{k}}^- - E_{\mathbf{k}}^+}$. Here, $\tilde{E}_{\mathbf{k}} = \sqrt{t_{x,\mathbf{k}}^2 + t_{z,\mathbf{k}}^2 + \bar{\lambda}_{\mathbf{k}}^2}$ are the eigenvalues of H_1 and the eigenvalues $E_{\mathbf{k}}^{\pm} = \varepsilon_{0,\mathbf{k}} \pm \tilde{E}_{\mathbf{k}}$ correspond the full Hamiltonian in Eq. (2) of the main text. Note that the coefficients s_3 , s_4 and s_5 vanish for higher-symmetry groups.

S2. FREE ENERGY INVARIANTS COUPLING MAGNETIZATION AND NÉEL ORDER

As discussed in the main text, a bilinear coupling between the magnetization and the Néel order exists if the direct product $\Gamma_A \otimes \Gamma_A \otimes \Gamma_N$ contains the IR transforming trivially under all point group operations, where Γ_A is the axial vector irreducible representation (IR) and Γ_N is the IR denoting the symmetry of the spin splitting. Equivalently, there is a free energy invariant if $\Gamma_A \otimes \Gamma_A$ contains Γ_N . In Table S1 we detail the axial vector IR for the different point groups.

As an example, we consider the point group D_{4h} . In this case, $\Gamma_A = E_g \oplus A_{2g}$, and therefore $\Gamma_A \otimes \Gamma_A = 3A_{1g} \oplus 2E_g \oplus (E_g \otimes E_g)$. Neither A_{1g} or E_g belong to Γ_N (see Table I in the main text), so the invariants can only arise from $E_g \otimes E_g = A_{1g} \oplus A_{2g} \oplus B_{1g} \oplus B_{2g}$. Hence, for each of $\Gamma_N = A_{2g}, B_{1g}, B_{2g}$ there is an allowed bilinear coupling. To illustrate how to obtain the form of the invariant, we focus on the case $\Gamma_N = B_{2g}$. The magnetization \vec{M} belongs to the axial vector IR, and therefore transforms like the spin Pauli matrices, $(M_x, M_y, M_z) \sim (\sigma_x, \sigma_y, \sigma_z)$,

Table S1. Axial vector irreducible representation Γ_A and antisymmetric direct product $[\Gamma_A \otimes \Gamma_A]_-$ for all point groups considered in Table I of the main text.

P	C_{2h}	D_{2h}	C_{4h}	D_{4h}	D_{3d}	C_{6h}	D_{6h}	O_h
Γ_A	$B_g \oplus A_g$	$B_{1g} \oplus B_{2g} \oplus B_{3g}$	$A_g \oplus E_g$	$E_g \oplus A_{2g}$	$A_{2g} \oplus E_g$	$A_g \oplus E_{1g}$	$A_{2g} \oplus E_{1g}$	T_{1g}
$[\Gamma_A \otimes \Gamma_A]_-$	B_g	$B_{1g} \oplus B_{2g} \oplus B_{3g}$	A_g	A_{2g}	A_{2g}	A_g	A_{2g}	T_{1g}

while for the Néel order $(N_x, N_y, N_z) \sim \tau_z(\sigma_x, \sigma_y, \sigma_z)$ (see Eq. (3) in the main text). Since τ_z transforms like the crystal asymmetric hopping $t_{z,\mathbf{k}}$ it belongs to the IR Γ_N . Thus, in our particular example $\Gamma_N = B_{2g} \sim k_x k_y$ and $(\sigma_x, \sigma_y, \sigma_z) \sim (k_y k_z, k_x k_z, k_x k_y (k_x^2 - k_y^2))$. As a consequence, the only allowed invariant corresponds to $M_x N_y + M_y N_x$. Following this procedure, we have identified the invariants for the different point groups and symmetries of the altermagnetic spin splitting listed in Table I in the main text.

As seen from Table I in the main text, there are some cases where a bilinear coupling between \vec{M} and \vec{N} is not symmetry allowed. For instance, focusing on the point group D_{6h} , the axial IR corresponds to $\Gamma_A = A_{2g} \oplus E_{1g}$. Therefore, $\Gamma_A \otimes \Gamma_A = A_{1g} \oplus 2E_{1g} \oplus (E_{1g} \otimes E_{1g})$, with $E_{1g} \otimes E_{1g} = A_{1g} \oplus A_{2g} \oplus E_{2g}$, which implies that there is only a bilinear coupling for $\Gamma_N = A_{2g}$ and not for $\Gamma_N = B_{1g}, B_{2g}$. Similarly, a bilinear coupling is not allowed for C_{6h} and O_h . Consequently, to obtain the lowest-order invariant we have derived the coupling between \vec{M} and \vec{N} to third order. In these cases, an invariant is obtained if $(\Gamma_A \otimes \Gamma_A \otimes \Gamma_A)_{\text{sym}} \otimes \Gamma_A$ contains Γ_N , where sym denotes the symmetric product of three IRs [1]. The invariant is included in Table I of the main text.

S3. ANALYTIC EXPRESSION FOR THE COEFFICIENTS IN THE FREE ENERGY FROM MICROSCOPIC MODELS

In this section, we provide the analytic expressions for the coefficients a_N , b_N and a_M entering in the free energy in Eq. (1) of the main text using the microscopic model in Eq. (2) and the perturbation in Eq. (3). In the main text, we focus on the interplay between the magnetization and the Néel order, examining the expression for the c_{ij} coefficient, in addition to the coefficients s_1 and s_2 , which determine the magnetic anisotropy energy due to the effect of SOC.

We start by deriving an expression for the free energy density from the partition function Z as

$$\begin{aligned} F &= -\frac{1}{\beta} \log Z = -\frac{1}{\beta} \log \left[\int dcd\bar{c} \exp(-cG^{-1}\bar{c}) \right] = -\frac{1}{\beta} \log \det(G^{-1}) = -\frac{1}{\beta} \sum_{i\omega_n} \text{Tr} \log(G^{-1}) \\ &= -\frac{1}{\beta} \sum_{i\omega_n} \text{Tr} \log(G_0^{-1} + H') = -\frac{1}{\beta} \sum_{i\omega_n} \text{Tr} [\log(G_0^{-1}) + \log(1 + G_0 H')] \\ &= -\frac{1}{\beta} \sum_{i\omega_n} \text{Tr} \log G_0^{-1} + \frac{1}{2\beta} \sum_{i\omega_n} \text{Tr}((G_0 H')^2) + \frac{1}{4\beta} \sum_{i\omega_n} \text{Tr}((G_0 H')^4), \end{aligned}$$

where G is the full Green's function, G_0 is the bare Green's function and H' is the perturbation to the normal-state Hamiltonian written in Eq. (3) of the main text, including the Néel order \vec{N} and the induced magnetization \vec{M} . In addition, $\beta = 1/k_B T$ and ω_n corresponds to the Matsubara frequency.

Hence, the second and fourth order corrections to the normal state free energy when the magnetic order sets in are evaluated from

$$F^{(2)} = \frac{1}{2\beta} \sum_{i\omega_n} \text{Tr}[G_0(\mathbf{k}, i\omega_n) H' G_0(\mathbf{k}, i\omega_n) H'], \quad (\text{S5})$$

$$F^{(4)} = \frac{1}{4\beta} \sum_{i\omega_n} \text{Tr}[(G_0(\mathbf{k}, i\omega_n) H')^4]. \quad (\text{S6})$$

The corresponding diagrammatic representation is illustrated in Fig. S1(a) and (b), respectively, where \vec{a} can denote both order parameters \vec{N} and \vec{M} . The bare Green's function projected to the band basis corresponds to

$$G_0(\mathbf{k}, i\omega_n) = \sum_{a=\pm} G_0^a(\mathbf{k}, i\omega_n) |u_{\mathbf{k}}^a\rangle \langle u_{\mathbf{k}}^a|, \quad (\text{S7})$$

where $G_0^{(\pm)}(\mathbf{k}, i\omega_n) = \frac{1}{i\omega_n - (\varepsilon_{0,\mathbf{k}} \pm \tilde{E}_{\mathbf{k}})}$ denotes the Green's function in the band basis, with the two-fold degenerate eigenenergies $E_{\mathbf{k}}^{\pm} = \varepsilon_{0,\mathbf{k}} \pm \tilde{E}_{\mathbf{k}}$ where $\tilde{E}_{\mathbf{k}} = \sqrt{t_{x,\mathbf{k}}^2 + t_{z,\mathbf{k}}^2 + \tilde{\lambda}_{\mathbf{k}}^2}$ are the eigenenergies of $H_1 = t_{x,\mathbf{k}}\tau_x + t_{z,\mathbf{k}}\tau_z + \tau_y \tilde{\lambda}_{\mathbf{k}} \cdot \vec{\sigma}$. With this, we construct the projection operator [2, 3]

$$P_{\mathbf{k}}^a = |u_{\mathbf{k}}^a\rangle \langle u_{\mathbf{k}}^a| = \frac{1}{4} \left(\mathbf{1} + \frac{H_1}{\pm \tilde{E}_{\mathbf{k}}} \right) \quad (\text{S8})$$

from sublattice basis onto band a at wavevector \mathbf{k} .

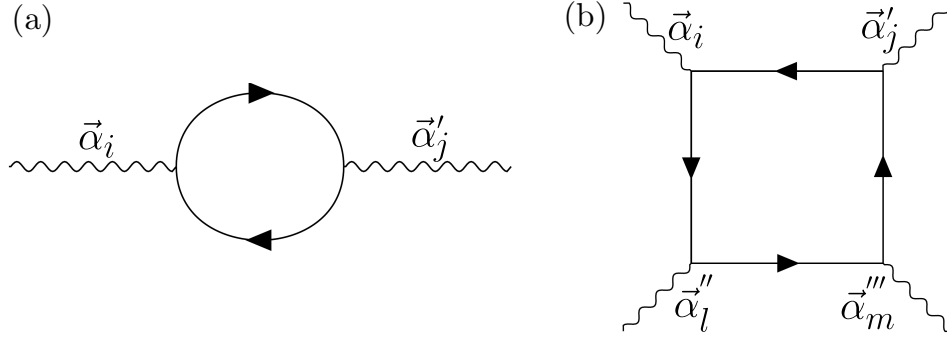


Figure S1. (a) Second-order and (b) fourth-order diagrams contributing to the free energy expansion where $\vec{\alpha}_i$, $\vec{\alpha}'_j$, $\vec{\alpha}''_l$ and $\vec{\alpha}'''_m$ can denote the components of the two magnetic orders \vec{M} and \vec{N} .

We focus first on the term coupling the two Néel order parameters \vec{N} corresponding to the coefficient a_N in the free energy, obtaining

$$F_N^{(2)} = \frac{\vec{N}^2}{\beta} \sum_{i\omega_n} \text{Tr} \left[\sum_{a,b} G^a(\mathbf{k}, i\omega_n) G^b(\mathbf{k}, i\omega_n) \tau_z |u_{\mathbf{k}}^a\rangle \langle u_{\mathbf{k}}^a| \tau_z |u_{\mathbf{k}}^b\rangle \langle u_{\mathbf{k}}^b| \right], \quad (\text{S9})$$

where we have replaced the Green's function projected in the band basis (see Eq. (S7)) into Eq. (S5). Note that the trace is over all degrees of freedom, including \mathbf{k} and the Matsubara frequency $i\omega_n$. Using the projector operator written in Eq. (S8), the expression for the free energy can be simplified to

$$F_N^{(2)} = \frac{\vec{N}^2}{\beta} \sum_{\mathbf{k}, i\omega_n} \frac{1}{t_{x,\mathbf{k}}^2 + t_{z,\mathbf{k}}^2} \left(2t_{x,\mathbf{k}}^2 G^-(\mathbf{k}, i\omega_n) G^+(\mathbf{k}, i\omega_n) + t_{z,\mathbf{k}}^2 [(G^-(\mathbf{k}, i\omega_n))^2 + (G^+(\mathbf{k}, i\omega_n))^2] \right). \quad (\text{S10})$$

Hence, performing the Matsubara frequency sum we identify

$$a_N = \frac{1}{U} + 2 \sum_{\mathbf{k}} \frac{1}{t_{x,\mathbf{k}}^2 + t_{z,\mathbf{k}}^2} \left\{ t_{x,\mathbf{k}}^2 \frac{2[f(E_{\mathbf{k}}^-) - f(E_{\mathbf{k}}^+)]}{E_{\mathbf{k}}^- - E_{\mathbf{k}}^+} + t_{z,\mathbf{k}}^2 \left[\left. \frac{df(\varepsilon)}{d\varepsilon} \right|_{\varepsilon=E_{\mathbf{k}}^+} + \left. \frac{df(\varepsilon)}{d\varepsilon} \right|_{\varepsilon=E_{\mathbf{k}}^-} \right] \right\}, \quad (\text{S11})$$

with $f(E_{\mathbf{k}}^a)$ denoting the Fermi function evaluated for the energy band a . Here, $\frac{1}{U}$ is the bare bosonic contribution from the Hubbard–Stratonovich transformation. This expression reveals that the susceptibility depends on the competition between the inter-band term and the intra-band term, as discussed in Ref. [3], and this determines whether ferromagnetism or Néel order is stabilized. Additionally, it also shows that band degeneracies help stabilizing altermagnetism.

We can follow the same procedure to obtain the a_M coefficient by focusing on the magnetization term in the perturbation. Thus, the free energy now simply reads

$$F_M^{(2)} = \frac{\vec{M}^2}{\beta} \sum_{\mathbf{k}, i\omega_n} [(G^-(\mathbf{k}, i\omega_n))^2 + (G^+(\mathbf{k}, i\omega_n))^2]. \quad (\text{S12})$$

Similarly to the previous case, the expression for the coefficient corresponds to

$$a_M = \frac{1}{U} + 2 \sum_{\mathbf{k}} \left\{ \left. \frac{df(\varepsilon)}{d\varepsilon} \right|_{\varepsilon=E_{\mathbf{k}}^+} + \left. \frac{df(\varepsilon)}{d\varepsilon} \right|_{\varepsilon=E_{\mathbf{k}}^-} \right\}. \quad (\text{S13})$$

In contrast to Eq. (S11), this coefficient contains only an intra-band term.

Finally, we can use Eq. (S6) to derive an expression for the quartic contribution to the free energy from the microscopic model, which corresponds to the diagram in Fig. S1(b). In this case, the expression for the coefficient b_N

in the free energy expansion corresponds to

$$\begin{aligned}
b_N = 4 \sum_{\mathbf{k}} \frac{1}{(t_{x,\mathbf{k}}^2 + t_{z,\mathbf{k}}^2)^2} & \left\{ \frac{t_{x,\mathbf{k}}^4}{(E_{\mathbf{k}}^- - E_{\mathbf{k}}^+)^2} \left(f'(\varepsilon) \Big|_{\varepsilon=E_{\mathbf{k}}^+} + f'(\varepsilon) \Big|_{\varepsilon=E_{\mathbf{k}}^-} - 2 \frac{f(E_{\mathbf{k}}^-) - f(E_{\mathbf{k}}^+)}{E_{\mathbf{k}}^- - E_{\mathbf{k}}^+} \right) + \frac{t_{z,\mathbf{k}}^4}{12} \left(f'''(\varepsilon) \Big|_{\varepsilon=E_{\mathbf{k}}^+} + f'''(\varepsilon) \Big|_{\varepsilon=E_{\mathbf{k}}^-} \right) \right. \\
& \left. + \frac{t_{x,\mathbf{k}}^2 t_{z,\mathbf{k}}^2}{E_{\mathbf{k}}^- - E_{\mathbf{k}}^+} \left(f''(\varepsilon) \Big|_{\varepsilon=E_{\mathbf{k}}^+} + f''(\varepsilon) \Big|_{\varepsilon=E_{\mathbf{k}}^-} - \frac{4}{E_{\mathbf{k}}^- - E_{\mathbf{k}}^+} \left[f'(\varepsilon) \Big|_{\varepsilon=E_{\mathbf{k}}^+} + f'(\varepsilon) \Big|_{\varepsilon=E_{\mathbf{k}}^-} \right] + 8 \frac{f(E_{\mathbf{k}}^-) - f(E_{\mathbf{k}}^+)}{(E_{\mathbf{k}}^- - E_{\mathbf{k}}^+)^2} \right) \right\}. \tag{S14}
\end{aligned}$$

S4. SOC-ENABLED QUASI-SYMMETRY

In this section, we provide general quasi-symmetry criteria beyond what is used in the main text. The quasi-symmetry criteria comes from the following properties in the normal-state Hamiltonian. In the normal-state band projector and Green's function (Eq. (S8)), the SOC-linear contribution appears as a linear combination of the three SOC terms. Cross-terms like $\sqrt{\lambda_x \lambda_y}$ are absent here. Consequently, any quantities derived from the normal-state Green's function should exhibit the same behavior. In other words, the SOC-linear contributions to any Landau parameters and any linear response coefficients are always expressed as a linear combination of $\lambda_{x,y,z}$. This property is consistent across all the minimal models used in this study.

A. Quasi-symmetry used in the main text

The λ_x linear contribution, specifically, should then exist by itself, even when the other two SOC terms are taken to be exactly zero. When setting the other two SOC terms to zero, the resulting normal-state Hamiltonian gains additional symmetries: spin-rotational symmetries of arbitrary angles along the x -axis. If a Landau term is odd under any of these additional quasi-symmetries, then the corresponding Landau coefficient cannot host pure λ_x contribution, including λ_x^1 , λ_x^2 , λ_x^3 and so on. Similarly, spin rotational symmetry along the y - (or z)-axis can be used to rule out pure λ_y (or λ_z) contributions. If a Landau coefficient has no pure $\lambda_{x,y,z}$ contributions, then it must be at least quadratic in SOC.

B. General quasi-symmetry

The quasi-symmetry criteria described above provide a sufficient, but not necessary, condition to eliminate SOC-linear contributions. These criteria exclude not only SOC-linear terms such as $\lambda_{x,y,z}$ but also any contributions involving pure λ_i terms, like λ_x^3 . However, if a Landau coefficient's leading contribution is λ_x^3 , the quasi-symmetry argument above cannot confirm the absence of SOC-linear contributions. To address this, we develop a more general quasi-symmetry criterion specifically aimed at identifying SOC-linear contributions.

As an example, consider the Landau term $M_x N_x - M_y N_y$, which is relevant for the site symmetry B_{1g} in D_{4h} . We aim to demonstrate the absence of SOC-linear contributions to this coefficient. Based on the properties of the normal-state band projector, checking for λ_x -linear contributions reduces to analyzing the coefficient of $(M_x N_x - M_y N_y) M_x O_x$ in the absence of any SOC. The presence of a λ_x -linear contribution would manifest through the inclusion of an additional $M_x O_x$ factor. Importantly, no further SOC terms are included in this analysis. For completeness, we also account for a factor O_x from the real-space component of the SOC λ_x , though this will not influence the subsequent discussion.

The absence of SOC leads to arbitrary spin-rotational symmetry. The term $(M_x N_x - M_y N_y) M_x$ is odd under spin rotation C_{2y}^{spin} , so it must vanish. This implies the absence of λ_x -linear contribution to $(M_x N_x - M_y N_y)$. Similarly, to check the λ_y -linear contribution, we need to analyze $(M_x N_x - M_y N_y) M_y$ in the absence of any SOC. The term $(M_x N_x - M_y N_y) M_y$ is odd under spin rotation C_{2x}^{spin} , implying the absence of λ_y -linear contribution to $(M_x N_x - M_y N_y)$. For the λ_z -linear contribution, we need to analyze $(M_x N_x - M_y N_y) M_z$. This term is odd under C_{2x}^{spin} , preventing the λ_z -linear contribution to $(M_x N_x - M_y N_y)$. Therefore, $M_x N_x - M_y N_y$ has no SOC-linear contributions.

For completeness, let us also consider the term $M_z N_y^3$, which is relevant for the site symmetry B_{1g} in D_{6h} . The absence of λ_y and λ_z contributions follows from the same quasi-symmetry argument in the main text, where C_{2y}^{spin} (or C_{2z}^{spin}) rules out pure- λ_y (or λ_z) contributions. However, for λ_x , the quasi-symmetry argument in the main text

is insufficient because $M_z N_y^3$ is not odd under any spin rotation along x . Instead, the more general quasi-symmetry argument applies. Specifically, we analyze the Landau term $M_z N_y^3 M_x$. This term is odd under C_{4y}^{spin} , ruling out the λ_x -linear contribution to the coefficient of $M_z N_y^3$. Numerical study reveals a λ_x^3 contribution to this coefficient.

These examples demonstrate that SOC-linear contributions are possible only if the corresponding term forms a component of a spin vector. For instance, $M_x N_y - M_y N_x$ is the z -component of $\mathbf{M} \times \mathbf{N}$. Since $(\mathbf{M} \times \mathbf{N}) \cdot \mathbf{M}$ is allowed under arbitrary spin-rotational symmetry, $M_x N_y - M_y N_x$ can have a λ_z -linear coefficient. This analysis can be extended to other types of SOC dependence. For example, to check for a $\lambda_x \times \lambda_y$ contribution to the coefficient of a Landau term O , one can analyze the coefficient of $OM_x M_y$ under arbitrary spin rotations.

S5. SECONDARY ORDER PARAMETERS

When a primary order parameter sets in, secondary order parameters are also induced by symmetry. As seen from Eq. (9) of the main text, these secondary order parameters can induce a finite coupling between the Néel order \vec{N} and the magnetization \vec{M} . In this section, we focus on the tetragonal example with point group $P = D_{4h}$ and a symmetry for the spin splitting belonging to $\Gamma_N = B_{2g} \sim k_x k_y$, which is relevant for the rutile lattice (SG 136), and detail the form of the allowed secondary order parameters.

Since in this case M_y and N_x transform like σ_y , $N_x \sim \tau_z \sigma_x$ can induce M_y through 10 different secondary order parameters breaking time-reversal symmetry: $\sin k_x \sin k_y \tau_0 \sigma_x$, $\sin k_x \sin k_y \tau_z \sigma_y$, $\sin k_y \sin k_z \tau_0 \sigma_z$, $\cos \frac{k_x}{2} \sin \frac{k_y}{2} \sin \frac{k_z}{2} \tau_x \sigma_z$, $\sin k_x \sin k_z \tau_z \sigma_z$, $\sin k_y \sin k_z (\cos k_x - \cos k_y) \tau_0 \sigma_z$, $\sin k_x \sin k_z (\cos k_x - \cos k_y) \tau_z \sigma_z$, $(\cos k_x - \cos k_y) \tau_z \sigma_x$, $(\cos k_x - \cos k_y) \tau_0 \sigma_y$, and $\cos \frac{k_x}{2} \sin \frac{k_y}{2} \sin \frac{k_z}{2} \tau_y$. Remarkably, the last one corresponds to a pure orbital current state that couples to the Néel order, but there are other orders with different spin textures. Notably, $(\cos k_x - \cos k_y) \tau_z \sigma_x$ is able to couple to $\tau_z \sigma_x$ with a coefficient quadratic in SOC and it also couples to $\tau_0 \sigma_y$ with a coefficient linear in SOC.

Among them, quadratic SOC dependence of the FM spin moment can be obtained through 4 secondary order parameters: $\sin k_x \sin k_y \tau_0 \sigma_x$, $\sin k_x \sin k_y \tau_z \sigma_y$, $\cos \frac{k_x}{2} \sin \frac{k_y}{2} \sin \frac{k_z}{2} \tau_x \sigma_z$, and $\cos \frac{k_x}{2} \sin \frac{k_y}{2} \sin \frac{k_z}{2} \tau_y$. Other secondary order parameters lead to cubic SOC dependence of the FM spin moment.

S6. HOPPING PARAMETERS AND SOC FOR THE RUTILE LATTICE AND FeSb₂

The general form for the normal-state Hamiltonian describing altermagnetism is given in Eq. (2) of the main text. In Tables S2 - S3 we detail the relevant form for the hoppings and spin-orbit coupling for the rutile lattice (SG 136) and FeSb₂ (SG 58) used to obtain the band structures and the magnetizations as a function of the SOC strength shown in Fig. (2) of the main text.

In order to estimate the SOC for FeSb₂, we perform DFT calculations using Wien2k [4] (SG 58, $a = 5.8379\text{\AA}$, $b = 6.5248\text{\AA}$, $c = 3.1811\text{\AA}$, internal position $(x, y, z) = (0.20094827, 0.35723599, 0)$ for Sb on Wyckoff position 4g), and read off the splittings induced by the spin-orbit terms at $\mathbf{k}_1 = (\pi, 0, \pi)$ where $t_{x, \mathbf{k}_1} = t_{z, \mathbf{k}_1} = \lambda_{y, \mathbf{k}_1} = \lambda_{z, \mathbf{k}_1} = 0$ and the splitting is solely induced by $\lambda_{x, \mathbf{k}_1} = \lambda_x$. Similarly, at $\mathbf{k}_2 = (0, \pi, \pi)$, we have $t_{x, \mathbf{k}_2} = t_{z, \mathbf{k}_2} = \lambda_{x, \mathbf{k}_2} = \lambda_{z, \mathbf{k}_2} = 0$ and the splitting is given by $\lambda_{y, \mathbf{k}_2} = \lambda_y$. Finally, for λ_z we use the self-consistently converged densities in the DFT calculation with SOC, but calculate the eigenenergies without including the SOC perturbatively. The energy shift ΔE of the band positions with and without SOC at the Γ point is given by $\Delta E = \sqrt{t_8^2 + \lambda_z^2} - |t_8|$ since the other components of the SOC vanish. Using that $t_8 = 0.15$ eV, we obtain $\vec{\lambda}_0 = (2.7, 6.6, 75)$ meV as used for the calculations in the main text.

Table S2. Tight-binding hoppings and SOC entering in the minimal model in Eq. (2) of the main text relevant for the rutile lattice and FeSb₂, as identified in Ref. [3]. The hopping and SOC parameters are detailed in Table S3.

	Rutile lattice	FeSb ₂
$t_{x, \mathbf{k}}$	$t_8 \cos \frac{k_x}{2} \cos \frac{k_y}{2} \cos \frac{k_z}{2}$	
$t_{z, \mathbf{k}}$	$t_6 \sin k_x \sin k_y + t_7 \sin k_x \sin k_y \cos k_z$	
$\lambda_{x, \mathbf{k}}$	$\lambda \sin \frac{k_z}{2} \sin \frac{k_x}{2} \cos \frac{k_y}{2}$	$\lambda_x \sin \frac{k_z}{2} \sin \frac{k_x}{2} \cos \frac{k_y}{2}$
$\lambda_{y, \mathbf{k}}$	$-\lambda \sin \frac{k_z}{2} \sin \frac{k_y}{2} \cos \frac{k_x}{2}$	$\lambda_y \sin \frac{k_z}{2} \sin \frac{k_y}{2} \cos \frac{k_x}{2}$
$\lambda_{z, \mathbf{k}}$	$\lambda_z \cos \frac{k_z}{2} \cos \frac{k_x}{2} \cos \frac{k_y}{2} (\cos k_x - \cos k_y)$	$\lambda_z \cos \frac{k_z}{2} \cos \frac{k_x}{2} \cos \frac{k_y}{2}$
$\varepsilon_{0, \mathbf{k}}$	$t_1 (\cos k_x + \cos k_y) + t_2 \cos k_z + t_3 \cos k_x \cos k_y$ $+ t_4 (\cos k_x + \cos k_y) \cos k_z$ $+ t_5 \cos k_x \cos k_y \cos k_z - \mu$	$t_{1,x} \cos k_x + t_{1,y} \cos k_y + t_2 \cos k_z$ $+ t_3 \cos k_x \cos k_y + t_{4,x} \cos k_x \cos k_z$ $+ t_{4,y} \cos k_y \cos k_z + t_5 \cos k_x \cos k_y \cos k_z - \mu$

Table S3. Tight-binding hopping parameters in units of eV found in Ref. [3] used to obtain the band structures in Fig. (1) of the main text and Figs. S4-S5. The SOC parameters estimated from DFT results.

RuO ₂	t_1	t_2	t_3	t_4	t_5	t_6	t_7	t_8	μ	λ	λ_z			
	-0.05	0.7	0.5	-0.15	-0.4	-0.6	0.3	1.7	0.25	0.05	0.17			
FeSb ₂	$t_{1,x}$	$t_{1,y}$	t_2	t_3	$t_{4,x}$	$t_{4,y}$	t_5	t_6	t_7	t_8	μ	λ_x	λ_y	λ_z
	-0.1	-0.05	-0.05	0.06	0.1	0.05	-0.05	0.05	-0.1	0.15	-0.12	0.0027	0.0066	0.075

For RuO₂, we use the same procedure, i.e. a DFT calculation using Wien2k [4] (SG 136, $a = 4.4825\text{\AA}$, $c = 3.1113\text{\AA}$, internal position $(x, y, z) = (0.30544216, 0.30544216, 0)$ for O on Wyckoff position 4f, and Ru on Wyckoff position 2a), once with spin-orbit coupling and once without it. We then find λ at the point $\mathbf{k}_3 = (\pi, 0, \pi)$ where all but $\lambda_{x,\mathbf{k}}$ vanish. λ_z is here identified at the point $\mathbf{k}_4 = (\frac{\pi}{2}, 0, 0)$ where $\Delta E = \frac{1}{\sqrt{2}}(\sqrt{t_8^2 + \lambda_z^2} - |t_8|)$. For RuO₂ we then obtain $\vec{\lambda}_0 = (0.05, 0.05, 0.17)$ eV.

S7. GENERAL EXPRESSIONS FOR THE BERRY CURVATURE

In the presence of SOC, the Néel order \vec{N} induces a FM order \vec{M} . Focusing on the previous cases of the rutile lattice and FeSb₂, the free energy invariant corresponds to $M_x N_y + M_y N_x$. Therefore, an in-plane Néel order $\vec{N} = (N_x, 0, 0)$ induces a magnetization $\vec{M} = (0, M_y, 0)$. In the presence of these orders, the Hamiltonian without including the dispersion corresponds to

$$H = t_{x,\mathbf{k}}\tau_x + t_{z,\mathbf{k}}\tau_z + \tau_y \vec{\lambda}_{\mathbf{k}} \cdot \vec{\sigma} + M_y \sigma_y + N_x \tau_z \sigma_x, \quad (\text{S15})$$

with

$$E_{\alpha=\pm, \beta=\pm} = \alpha \left(N_x^2 + M_y^2 + \vec{\lambda}_{\mathbf{k}}^2 + t_{x,\mathbf{k}}^2 + t_{z,\mathbf{k}}^2 + \beta 2 \sqrt{N_x^2 (\lambda_{z,\mathbf{k}}^2 + \lambda_{y,\mathbf{k}}^2 + t_{z,\mathbf{k}}^2) + M_y^2 (\lambda_{y,\mathbf{k}}^2 + t_{z,\mathbf{k}}^2 + t_{x,\mathbf{k}}^2) - 2N_x M_y \lambda_{z,\mathbf{k}} t_{x,\mathbf{k}}} \right)^{1/2}. \quad (\text{S16})$$

The general lowest-order expression for the Berry curvature is given by [2]

$$\begin{aligned} \Omega_{\alpha,\beta,ij} = \sum_{m,n=i,j} \varepsilon_{mn} & \left[\frac{3M_y}{8E_2} \left(\frac{\beta(N_x^2 + M_y^2)}{3E_2^2} + \frac{\beta N_x^2(N_x^2 + t_{x,\mathbf{k}}^2 + 2M_y^2) + M_y^4}{E_{\alpha\beta}^2 E_2^2} + \frac{2(N_x^2 + M_y^2)}{E_{\alpha\beta}^2 E_2} + \frac{\beta}{E_{\alpha\beta}^2} \right) \right. \\ & (\lambda_{y,\mathbf{k}} \partial_m t_{x,\mathbf{k}} \partial_n t_{z,\mathbf{k}} + t_{x,\mathbf{k}} \partial_m t_{z,\mathbf{k}} \partial_n \lambda_{y,\mathbf{k}} + t_{z,\mathbf{k}} \partial_m \lambda_{y,\mathbf{k}} \partial_n t_{x,\mathbf{k}}) \\ & + \frac{N_x t_{z,\mathbf{k}}}{8E_{\alpha\beta}^3} \left(\frac{\beta(N_x^2 t_{z,\mathbf{k}}^2 + M_y^2(t_{x,\mathbf{k}}^2 + t_{z,\mathbf{k}}^2))}{E_2^3} + \frac{3\beta}{E_2} \right) (\lambda_{x,\mathbf{k}} \partial_m t_{x,\mathbf{k}} \partial_n t_{z,\mathbf{k}} + t_{x,\mathbf{k}} \partial_m t_{z,\mathbf{k}} \partial_n \lambda_{x,\mathbf{k}} + t_{z,\mathbf{k}} \partial_m \lambda_{x,\mathbf{k}} \partial_n t_{x,\mathbf{k}}) \\ & \left. + \frac{N_x}{8E_{\alpha\beta}^3} \left(\frac{3N_x^2 t_{z,\mathbf{k}}^2 + 3M_y^2(t_{x,\mathbf{k}}^2 + t_{z,\mathbf{k}}^2)}{E_2^2} + 1 \right) (\partial_m \lambda_{x,\mathbf{k}} \partial_n t_{x,\mathbf{k}}) \right], \quad (\text{S17}) \end{aligned}$$

where we introduced

$$E_2 = \sqrt{N_x^2 (\lambda_{z,\mathbf{k}}^2 + \lambda_{y,\mathbf{k}}^2 + t_{z,\mathbf{k}}^2) + M_y^2 (\lambda_{y,\mathbf{k}}^2 + t_{z,\mathbf{k}}^2 + t_{x,\mathbf{k}}^2) - 2N_x M_y \lambda_{z,\mathbf{k}} t_{x,\mathbf{k}}}, \quad (\text{S18})$$

which has units of energy squared. When $M_y = 0$, Eq. (S17) reduces to

$$\begin{aligned} \Omega_{\alpha,\beta,ij} = \frac{1}{8E_{\alpha\beta}^3} \sum_{m,n=i,j} \varepsilon_{mn} & \left[\left(N_x + \frac{3N_x t_{z,\mathbf{k}}^2}{E_1^2} + \frac{3\beta t_{z,\mathbf{k}}^2}{E_1} + \frac{\beta t_{z,\mathbf{k}}^4}{E_1^3} \right) \partial_m \lambda_{x,\mathbf{k}} \partial_n t_{x,\mathbf{k}} + \left(\frac{3\beta \lambda_{x,\mathbf{k}} t_{z,\mathbf{k}}}{E_1} + \frac{\beta \lambda_{x,\mathbf{k}} t_{z,\mathbf{k}}^3}{E_1^3} \right) \partial_m t_{x,\mathbf{k}} \partial_n t_{z,\mathbf{k}} \right. \\ & \left. + \left(\frac{3\beta t_{x,\mathbf{k}} t_{z,\mathbf{k}}}{E_1} + \frac{\beta t_{x,\mathbf{k}} t_{z,\mathbf{k}}^3}{E_1^3} \right) \partial_m t_{z,\mathbf{k}} \partial_n \lambda_{x,\mathbf{k}} \right], \quad (\text{S19}) \end{aligned}$$

which includes SOC components in all direction and where now $E_1 = \sqrt{t_{z,\mathbf{k}}^2 + \lambda_{z,\mathbf{k}}^2 + \lambda_{y,\mathbf{k}}^2}$. For $\lambda_{y,\mathbf{k}} = \lambda_{z,\mathbf{k}} = 0$, this expression further reduces to Eq. (10) in the main text.

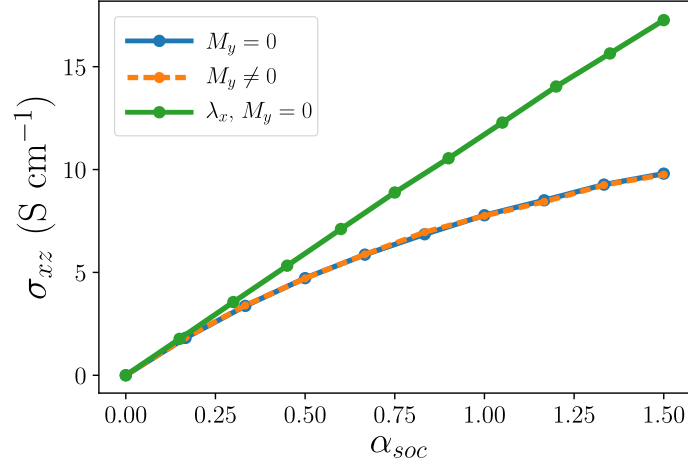


Figure S2. Hall conductivity as a function of SOC strength for RuO₂, considering the tight-binding model and parameters in Tables S2-S3. We take $\vec{\lambda} = \alpha_{soc}\vec{\lambda}_0$ with $\vec{\lambda}_0 = (0.05, 0.05, 0.17)$ eV and $N_x = 0.2$ eV. The orange (blue) line corresponds to the Berry curvature in Eq. (S17) (Eq. (S19)). The green line is obtained from the Berry curvature in Eq. (S19) considering only SOC in the x -direction.

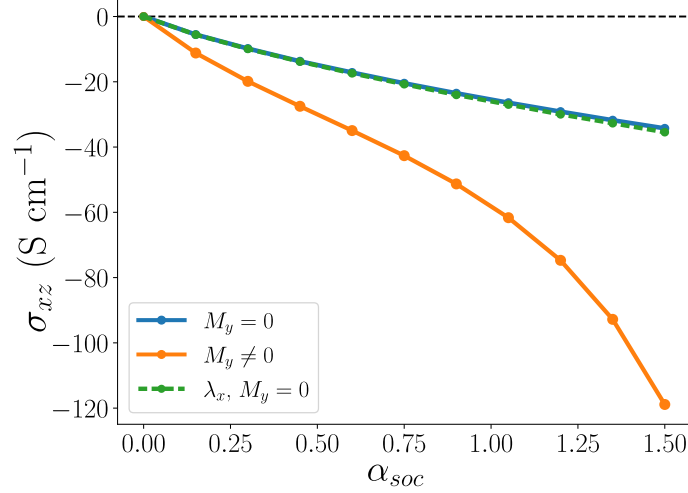


Figure S3. Hall conductivity as a function of SOC strength for FeSb₂, considering the tight-binding model and parameters in Tables S2-S3. We take $\vec{\lambda} = \alpha_{soc}\vec{\lambda}_0$ with $\vec{\lambda}_0 = (0.0027, 0.0066, 0.075)$ eV and $N_x = 0.05$ eV. The orange (blue) line corresponds to the Berry curvature in Eq. (S17) (Eq. (S19)). The green line is obtained from the Berry curvature in Eq. (S19) considering only SOC in the x -direction.

We have additionally considered the Berry curvature in the presence of only an in-plane M_y magnetization. In this case, Eq. (S17) reduces to

$$\Omega_{\alpha,\beta,ij}^{(M_y)} = \frac{\text{sgn}(M_y)\beta}{8\tilde{E}^3} \sum_{m,n=i,j} \varepsilon_{mn} \left[\left(1 + \frac{3}{E_{\alpha,\beta}^2} (\tilde{E}_y + \beta|M_y|)^2 \right) (t_{z,\mathbf{k}}\partial_m\lambda_{y,\mathbf{k}}\partial_n t_{x,\mathbf{k}} + t_{x,\mathbf{k}}\partial_m t_{z,\mathbf{k}}\partial_n \lambda_{y,\mathbf{k}} + \lambda_{y,\mathbf{k}}\partial_m t_{x,\mathbf{k}}\partial_n t_{z,\mathbf{k}}) \right], \quad (\text{S20})$$

and the Berry curvature is also linear in the SOC component parallel to the magnetization. In the previous expression, $\tilde{E}_y = \sqrt{t_{z,\mathbf{k}}^2 + t_{x,\mathbf{k}}^2 + \lambda_{y,\mathbf{k}}^2}$ and $E_{\alpha=\pm,\beta=\pm}$ is now Eq. (S16) in the case $N_x = 0$. The dispersion of the spin up and spin down bands is different in the presence of \vec{M} , and consequently this term also give rise to a finite AHE.

In Figs. S2-S3 we show the Hall conductivity for the rutile lattice and the FeSb₂ tight-binding models (see Tables S2-

S3), calculated from the Berry curvature as

$$\sigma_{ij} = -\frac{e^2}{\hbar} \int_{\text{BZ}} \frac{d\mathbf{k}}{(2\pi)^3} \sum_{\alpha,\beta} f_{\alpha,\beta}(\mathbf{k}) \Omega_{\alpha,\beta,ij}, \quad (\text{S21})$$

where $f_{\alpha,\beta}(\mathbf{k})$ is the Fermi-Dirac contribution of each band α, β . In the case of RuO₂ ($P = D_{4h}$, $\Gamma_N = B_{2g}$), see Fig. S2, Eqs. (S17) and (S19) yield almost the same result for the conductivity. Therefore, the induced magnetization for this tetragonal material does not give rise to a significant contribution to the anomalous Hall conductivity, as expected from Table I in the main text, since \vec{M} is induced to second (or higher order) in the SOC. In contrast, if we focus on the band structure inspired by FeSb₂ ($P = D_{2h}$, $\Gamma_N = B_{1g}$), the induced magnetization \vec{M} is allowed to linear order in SOC (see Table I in the main text) and may give rise to significant contributions to the anomalous Hall conductivity, as seen from Fig. S3.

S8. MAGNETIC ANISOTROPY ENERGY

In this section, we derive the expression for the magnetic anisotropy energy and examine the preferred direction using microscopic models relevant for the rutile lattice (SG 136) and FeSb₂ (SG 58). In the presence of the Néel order parameter and SOC the free energy is given by

$$F = s_x N_x^2 + s_y N_y^2 + s_z N_z^2. \quad (\text{S22})$$

In Eq. (1) of the main text we rewrite this expression in the form

$$F = s_0(N_x^2 + N_y^2 + N_z^2) + s_1(N_x^2 - N_y^2) + s_2(N_x^2 + N_y^2 - 2N_z^2), \quad (\text{S23})$$

so that the coefficients s_0 , s_1 and s_2 correspond to

$$\begin{aligned} s_0 &= \frac{1}{3}(s_x + s_y + s_z), \\ s_1 &= \frac{1}{2}(s_x - s_y), \\ s_2 &= \frac{1}{6}(s_x + s_y - 2s_z). \end{aligned} \quad (\text{S24})$$

The expression for the coefficients is derived from the following contribution of the free energy to second order (see Fig. S1(a)),

$$F_J^{(2)} = \frac{1}{2\beta} \sum_{i\omega_n} \text{Tr} \left[\sum_{a,b} G^a(\mathbf{k}, i\omega_n) G^b(\mathbf{k}, i\omega_n) \tau_z \vec{N} \cdot \vec{\sigma} P_{\mathbf{k}}^a \tau_z \vec{N} \cdot \vec{\sigma} P_{\mathbf{k}}^b \right], \quad (\text{S25})$$

where $G^a(\mathbf{k}, i\omega_n)$ and $P_{\mathbf{k}}^a$ are the Green's function and the projector operator defined in Eq. (S7) and Eq. (S8), respectively. In particular, we are concerned with the corrections due to SOC, and therefore we specifically analyze the trace

$$\begin{aligned} & \frac{1}{16} \text{Tr} \left[\tau_z \vec{N} \cdot \vec{\sigma} \tau_y \vec{\lambda}_{\mathbf{k}} \cdot \vec{\sigma} \tau_z \vec{N} \cdot \vec{\sigma} \tau_y \vec{\lambda}_{\mathbf{k}} \cdot \vec{\sigma} \right] \\ &= -\frac{1}{4} \left\{ N_x^2 (\lambda_{x,\mathbf{k}}^2 - \lambda_{y,\mathbf{k}}^2 - \lambda_{z,\mathbf{k}}^2) + N_y^2 (-\lambda_{x,\mathbf{k}}^2 + \lambda_{y,\mathbf{k}}^2 - \lambda_{z,\mathbf{k}}^2) + N_z^2 (-\lambda_{x,\mathbf{k}}^2 - \lambda_{y,\mathbf{k}}^2 + \lambda_{z,\mathbf{k}}^2) \right. \\ & \quad \left. + 4(N_x N_y \lambda_{x,\mathbf{k}} \lambda_{y,\mathbf{k}} + N_x N_z \lambda_{x,\mathbf{k}} \lambda_{z,\mathbf{k}} + N_y N_z \lambda_{y,\mathbf{k}} \lambda_{z,\mathbf{k}}) \right\}. \end{aligned} \quad (\text{S26})$$

From this expression, the general form of the free energy in Eq. (S1) directly follows. Focusing on orthorhombic or higher-symmetry groups, the form for the s_x , s_y and s_z coefficients in Eq. (S22) corresponds to

$$s_{i=\{x,y,z\}} = a_N - \sum_{\mathbf{k}} \frac{L(\mathbf{k})}{2\tilde{E}_{\mathbf{k}}^2} (\lambda_{i,\mathbf{k}}^2 - \sum_{j \neq i} \lambda_{j,\mathbf{k}}^2), \quad (\text{S27})$$

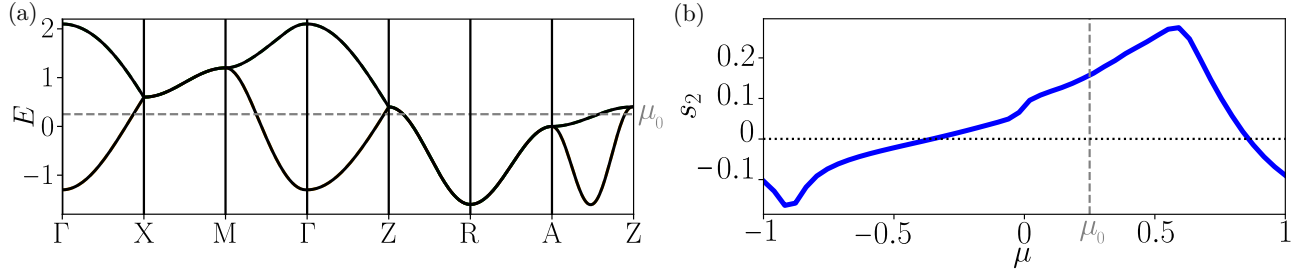


Figure S4. (a) Normal state band structure relevant for the rutile lattice (SG 136), using the tight-binding model in Table S2 and considering the hopping parameters in Table S3. (b) s_2 coefficient (see Eqs. (S23), (S28)) as a function of the chemical potential μ for the band structure shown in (a) and taking $T = 0.02$, $n_{\mathbf{k}} = 201^3$ and the SOC terms in Tables S2 - S3, displaying that the preferred direction for the Néel vector can switch by varying the Fermi energy.

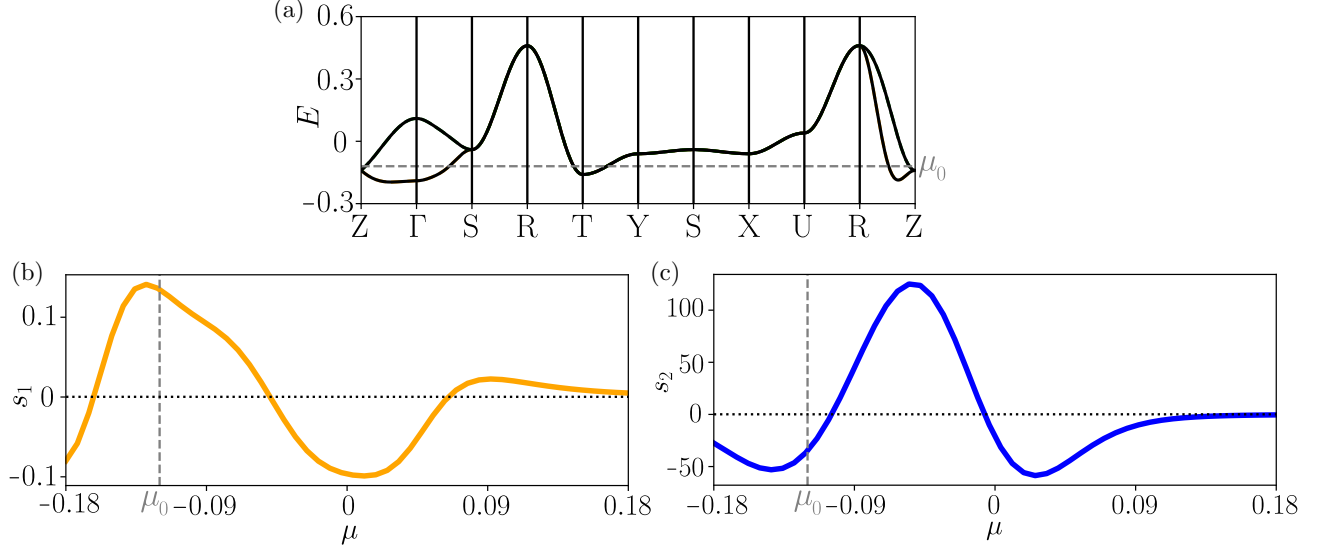


Figure S5. (a) Normal state band structure relevant for the FeSb₂ lattice (SG 58), using the tight-binding model in Table S2 and considering the hopping parameters in Table S3. (b)-(c) s_1 and s_2 coefficients (see Eqs. (S23), (S28)) as a function of μ for the band structure shown in (a) and taking $T = 0.02$, $n_{\mathbf{k}} = 201^3$ and the SOC terms in Tables S2 - S3, displaying that both the in-plane and out-of-plane preferred direction for the Néel vector can switch by varying the Fermi energy.

where the function $L(\mathbf{k})$ is defined in Eq. (8) of the main text. Thus, replacing this result in Eq. (S24),

$$\begin{aligned}
 s_0 &= a_N + \frac{1}{6} \sum_{\mathbf{k}} \frac{\lambda_{x,\mathbf{k}}^2 + \lambda_{y,\mathbf{k}}^2 + \lambda_{z,\mathbf{k}}^2}{\tilde{E}_{\mathbf{k}}^2} L(\mathbf{k}), \\
 s_1 &= -\frac{1}{2} \sum_{\mathbf{k}} \frac{\lambda_{x,\mathbf{k}}^2 - \lambda_{y,\mathbf{k}}^2}{\tilde{E}_{\mathbf{k}}^2} L(\mathbf{k}), \\
 s_2 &= -\frac{1}{6} \sum_{\mathbf{k}} \frac{\lambda_{x,\mathbf{k}}^2 + \lambda_{y,\mathbf{k}}^2 - 2\lambda_{z,\mathbf{k}}^2}{\tilde{E}_{\mathbf{k}}^2} L(\mathbf{k}).
 \end{aligned} \tag{S28}$$

In Fig. S4 and S5 we show the magnetic anisotropy coefficients for two different tight binding models. First, we focus on a model relevant for the rutile lattice (SG 136) with the band structure shown in Fig. S4(a). In this tetragonal case, the coefficient s_1 vanishes by symmetry, and s_2 determines the in-plane versus out-of-plane spin anisotropy. As seen from Fig. S4(b), for the chemical potential μ_0 the preferred direction for the Néel vector is out-of-plane. However, for a lower μ it changes to in-plane, which may be due to the competition between the Linhard function and the density of states in the function $L(\mathbf{k})$. Considering now the tight-binding model inspired by the FeSb₂ band structure, see Fig. S5(a), for this orthorhombic material both coefficients s_1 and s_2 are generally non-zero. For the chemical

potential μ_0 , Figs. S5(b)-(c) show that the preferred direction of the altermagnetic moments is along the y direction, but similar to the rutile case it can switch as a function of the Fermi energy.

-
- [1] Matthias Hecker, Anant Rastogi, Daniel F. Agterberg, and Rafael M. Fernandes, “Classification of electronic nematicity in three-dimensional crystals and quasicrystals,” *Phys. Rev. B* **109**, 235148 (2024).
 - [2] Ansgar Graf and Frédéric Piéchon, “Berry curvature and quantum metric in N -band systems: An eigenprojector approach,” *Phys. Rev. B* **104**, 085114 (2021).
 - [3] Mercè Roig, Andreas Kreisel, Yue Yu, Brian M. Andersen, and Daniel F. Agterberg, “Minimal models for altermagnetism,” *Phys. Rev. B* **110**, 144412 (2024).
 - [4] P. Blaha, K. Schwarz, G. K. Madsen, D. Kvasnicka, and J. Luitz, *WIEN2k an Augmented Plane Wave Plus Local Orbitals Program for Calculating Crystal Properties* (Technische Universität Wien, 2001).